Hindawi
Shock and Vibration
Volume 2022, Article ID 3820921, 9 pages
https://doi.org/10.1155/2022/3820921

Research Article

Experimental Study on SHPB Dynamic Mechanical Response in Different Damage Zones of Rock under Blast Load

Wenda Tang,[1] **Yuanyuan You**,[1] **Feng Hu**,[2,3] **Yuanyuan Bian**,[4] **Chenglong Xiao**,[1] **and Yijun Zhu**[2]

[1]*School of Mechanics and Civil Engineering, China University of Mining and Technology (Beijing), Beijing 100083, China*
[2]*Zhejiang Institute of Communications Co. Ltd., Hangzhou, Zhejiang 310030, China*
[3]*College of Civil Engineering and Architecture, Zhejiang University, Hangzhou, Zhejiang 310058, China*
[4]*China Academy of Building Research Co., Ltd., Beijing 100013, China*

Correspondence should be addressed to Wenda Tang; tang_wenda@126.com and Feng Hu; hf18810550150@outlook.com

Received 9 February 2022; Revised 22 February 2022; Accepted 24 February 2022; Published 27 March 2022

Academic Editor: Tao Meng

In this study, the damage characteristics of the slit charge pack along the rock slitting and the vertical slitting directions were investigated using green sandstone as the subject. Split-Hopkinson pressure bar (SHPB) experiments were performed on green sandstone, and the dynamic mechanical properties of rock specimen were analyzed in the slitting and vertical slitting directions. Based on the SHPB experiments of the rock specimens in different damage zones along the rock slitting and the vertical slitting directions combined with the fractal theory, the distribution pattern of rock fracture fragmentation was investigated at different positions in the kerf direction and vertical kerf direction. The results of this study show that the dynamic strength of the rock corresponds to the damage degree of the rock, which is greater in the direction of the slit than that in the perpendicular direction of the slit. In addition, the core at 150 mm distance from the blast hole perpendicular to the slit direction could easily bear the blast loads. The lumpiness distribution of rock specimens under impact load shows good statistical self-similarity. The evolution law of fractal dimension shows that with increasing distance from the core to the blast hole, the fractal dimension of the specimen after failure increases. The fractal dimension of the specimen perpendicular to the slit direction is greater than that of the specimen along the slit direction at the same distance.

1. Introduction

Rock blasting technology has found tremendous development and application; therefore, scientists and engineers working in this area have paid significant attention towards strategies to control the formation of blasting cracks more accurately and effectively protect the stability of surrounding rocks and slopes. In recent years, the directional control blasting technology of the slit charge pack is widely used and has shown remarkable effects in the engineering fields such as well tunneling, open-pit mine boundary, and foundation pit excavation; however, it is realized by the slitting charge, and thus the damage and destruction of the rock mass in the direction of the slit and perpendicular to the slit will bring unforeseen dangers to the safe construction and normal operation of the project. Therefore, in engineering practice, the degree of damage and dynamic mechanical response in the direction of the rock mass in the direction of the kerf and the direction of the vertical kerf provides a reliable basis for optimizing the design of engineering blasting parameters and blasting technology and improving the blasting effect. Therefore, it is very important to carry out research on the damage and dynamic mechanical response of slit charge blasting for surrounding rock stability control and blasting hazard prevention [1, 2].

In the 1970s, Fourney et al. [3–5] proposed forming directional fractures in rock mass using axially slit tubular charge in blast holes and developed a series of slit tubular charge tests, indicating that the fracture during the blasting process can be controlled by the slotted tube charge. In the

polymer and rock models, the fracture forms a fracture surface along the specified direction, inhibiting the generation of parasitic fracture cracks. The dynamic state of the stress and crack propagation revealed by the moving photoelastic recording has been described, and these results can be used to evaluate the effectiveness of blast control methods with slotted charge in controlling blast fracture [6]. Gao [7] performed numerical simulation on the propagation process of the blast stress wave and constitutive slit pipe of different materials based on the traditional theory and obtained the pressure in the blast hole wall along the slit direction and the vertical slit direction. In addition, the author further explored the blasting mechanism of the slit cartridge. Wang and Wei [8] pointed out that the slit width and shell thickness are the typical structural parameters that affect the directional propagation of cracks in slit pipes. When using No. 2 rock explosive in medium-hard limestone, the thickness of the plastic shell is 4.5 mm, and the uncoupling coefficient is $K = 1.33$, revealing the law of the effect of the slit width on the crack length and width. Yang et al. [9–12] used the method of dynamic moire and dynamic caustics to conduct a series of research on the distribution law of the stress field and the law of crack propagation in the slotted hole under blasting by changing the shape of the blast hole. The results show that the stress field is strengthened along the grooving direction and is more conducive to the directional propagation of cracks. The blasting parameters of the notch hole, namely, the notch angle, notch tip radius, and notch depth, are the main factors affecting the notch crack propagation.

The initiation, propagation, and arrest of cracks in blasting are mainly affected by the static pressure of the blasting gas. Yu et al. [13] prepared blasted sandstone blocks and the large fragments of the entire sandstone blocks as standard samples and carried out a series of Brazilian splitting tests to indirectly determine their tensile strength and analyze the distance from blasthole. Loading rates were 1.67×10^{-5} to 8.33×10^{-2} mm s^{-1}. The results show that the tensile strength of the specimen increases with increasing distance from the blast source and is close to the tensile strength of the undamaged rock mass, related with a positive exponential power function (0–1); the loading rate affects the tensile mechanics of the disc and this behavior is mainly manifested in the convergence of microscopic defects, the main bearing area of the specimen, and the energy absorption at the moment of specimen fracture. Both tensile strength and absorbed energy are positively and linearly related to the natural logarithm of the loading rate. Wang et al. explored the fractal characteristics of biotite under blasting loads [14] using a one-dimensional SHPB impact test to measure the dynamic compressive strength, failure form, fracture energy dissipation density, and other properties of rocks under different strain rates. The fractal characteristics of rock mass under different strains and different strain rates are determined by the sieving test, and the fractal dimension d of rock crushing is calculated. The results show that under different impact loads, the strain rate effect of rock is significant, and the dynamic compressive strength increases with increasing strain rate, following a power relationship. The higher the strain rate of rock is, the deeper the crushing degree is, and there is a power relationship between fractal dimension and rock crushing energy density. Although these research results contributed significantly in the directional control blasting mechanism and application of the slit charge, the dynamic mechanics of the rock in the direction of the rock slit and perpendicular to the direction of the slit charge under the action of the blast load of the slit charge [15–17] is rarely investigated. Relatively few studies have reported the properties and extent of the damage.

Slotting charge is widely used in coal mines and other sites, as it can significantly reduce the blasting damage of rock roadway and the phenomena of overbreak and underbreak caused by blasting. In this study, the Hopkinson pressure bar test system was used to study the dynamic mechanical properties and damage degree of the rock specimen in the direction of the slit and the direction perpendicular to the slit under the blasting load of the slit charge. The fractal theory was used to quantitatively describe the distribution law of rock fracture fragmentation at different positions in the kerf direction, and the vertical kerf direction was obtained.

2. Blasting Experiment of Slit Charge

2.1. Experimental Design. The blasting specimen was fabricated from an intake blue sandstone. The specimen has uniform lithology, fine-grained structure, and little macroscopically visible joints and fissures. The specimen size is $400 \times 400 \times 400$ mm^3, mainly composed of quartz, feldspar, and illite minerals. A blast hole with a depth of 320 mm and a diameter of 12 mm was drilled in the center of the specimen, and restraint was imposed using a steel plate as the passive confining pressure. The peripheral gap was filled with fine sand. The slit pipe is made of stainless steel, with an outer diameter of 8 mm, wall thickness of 1 mm, length of 315 mm, and slit width of 1.2 mm. The schematic diagram of the blasting specimen and the slit pipe is shown in Figure 1.

2.2. Failure Pattern of Specimen. The slotted tube was filled with 1300 mg lead azide elemental explosive, placed in the blast hole, and fixed in the slotting direction of the slotted tube in order for it to be parallel and perpendicular to the surrounding surface of the test piece. The blast hole was blocked, and the connecting wire was detonated. The results of the blasting test are shown in Figure 2, indicating that after blasting, the crack spreads along the slit, the specimen is divided into two parts, and the rupture surface is flat.

3. Core Hopkinson Pressure Bar Experiment

3.1. Core Drilling. Based on the blasting test results, continuous coring was carried out at the same distance in the slitting and vertical slitting directions. Five cores were taken at 150 mm, as shown in Figure 3(a). The cores in the vertical cutting direction are recorded as A1, A2, A3, A4, and A5, and those in the cutting direction are recorded as B1, B2, B3, B4, and B5, as shown in Figure 3(b). The unique side radial

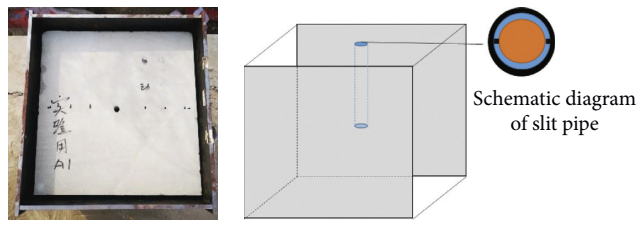

(a) (b)

Figure 1: Schematic diagram of the blasting specimen. (a) Green sandstone specimen. (b) Schematic diagram of slit pipe.

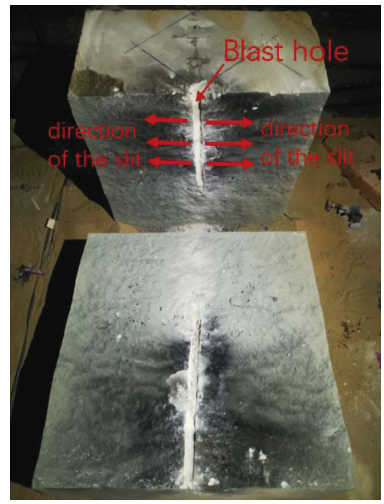

Figure 2: Blasting test results.

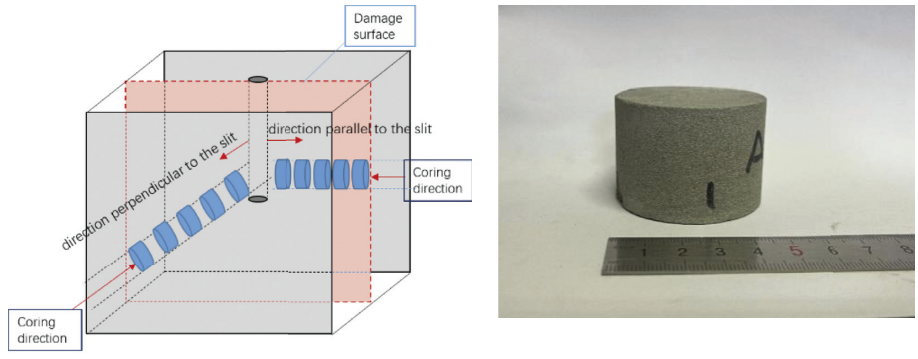

(a) (b)

Figure 3: Schematic diagram of the sample preparation process. (a) Schematic diagram of coring. (b) Schematic diagram of the test piece.

continuous coring method ensures that the coring samples are all at the same level in order to avoid the influence of different explosion damage effects caused by uneven charging.

3.2. Hopkinson Experiment System and Process. The Hopkinson pressure rod is essentially a simple elastic rod. A stress load $P(t)$ is applied to one end of the incident rod, and an elastic stress wave is induced in the incident rod. With the correct measurement method, applying the stress wave theory in one-dimensional rods, some specific parameters of the input and output ends of the specimen can be obtained, and the dynamic stress-strain, stress-time, and strain-time of the loading pulse can be obtained [18]. Figure 4 shows a schematic diagram of the Hopkinson pressure bar test method. The Hopkinson pressure rod test system consists of three parts: main equipment, a launch system, and a test system, comprising a cylinder, bullet, parallel light source, velocimeter, rubber shaper, incident rod, resistance strain gauge, bridge box, ultra-dynamic strain acquisition instrument, oscilloscope, computer, test piece, resistance strain gauge, bridge box, ultra-dynamic strain gauge, oscilloscope, computer, transmission rod, absorption rod, and damping

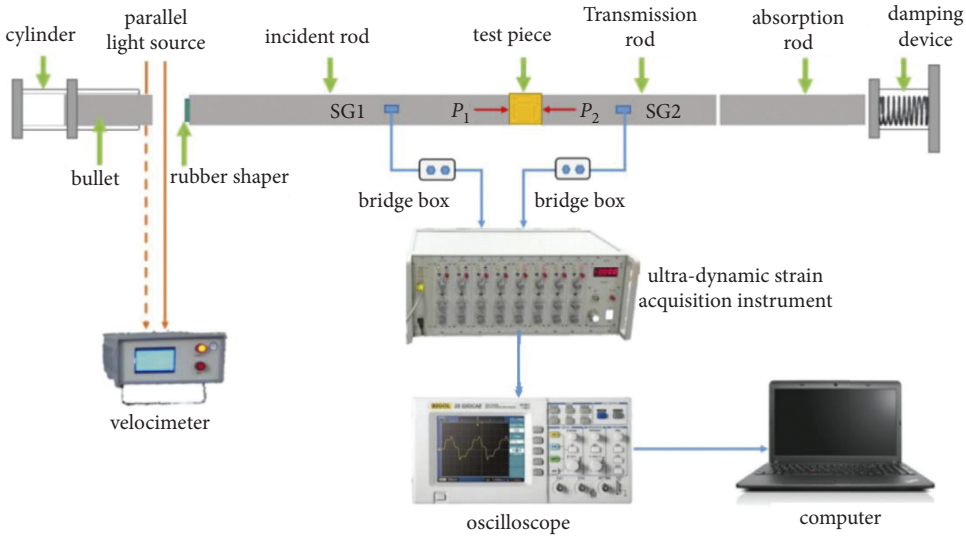

Figure 4: Schematic diagram of the Hopkinson pressure bar test method.

device, as shown from left to right in the figure. The pressure rod is made of high-strength alloy and the pressure rod and the actual contact surface are processed flat and parallel to avoid changing the shape of the stress wave [19, 20]. The uniaxial impact compression test was carried out using an SHPB steel rod with a diameter of 50 mm. The specification of the steel rod are as follows: elastic modulus, 210 GPa; density, 7800 kg/m^3; theoretical wave velocity, 5189 m/s; and the measured wave velocity is 5124 m/s. The impact rod is a tapered rod with a length of 0.3 m, and the lengths of the incident and transmission rods are 2.2 m and 1.5 m, respectively. During the test, the initial positions of the impact and the incident rods were unchanged to obtain the same impact rate, the core sample between the incident and the transmission rods was sandwiched, and Vaseline was evenly applied on the contact surface of the sample and the steel rod to reduce the friction. Then, the stress wave generating device was activated to hit the bullet with the elastic incident rod to generate a loading stress wave of a certain shape. Repeated tests were performed to ensure the accuracy of the test results.

4. Analysis of Test Results

4.1. Analysis of Sample Stress-Strain Relationship. The incident, transmitted, and reflected waves were measured by the strain gauges on the incident and the transmission rods, and the collected test data were processed by the three-wave method to calculate the stress and strain of the sample, which were then plotted to get the stress-strain relationship curves of the core samples taken in the cutting and vertical cutting directions, as shown in Figure 5.

The stress-strain relationship curves of the core sample shown in Figure 5 indicate that the yield strength of the core perpendicular to the cutting direction is greater than that of the core with the same distance from the blast hole. The stress-strain curve of the core at 150 mm distance from the blast hole perpendicular to the slitting direction is approximately consistent with the stress-strain curve of the blue sandstone core sample under no blast loading. Therefore, under the explosion of the slotted pipe, the damage degree in the direction is greater than that in the direction perpendicular to the cutting seam; however, the core with 150 mm from the blast hole perpendicular to the direction of the cutting seam is hardly affected by the explosion load.

The yield strength of the core samples in the direction of the slit and perpendicular to the slit increases with the distance from the blast hole. The damage degree of the specimen decreases continuously with increasing distance from the center of the blast hole irrespective of the direction of the slit or perpendicular to the direction of the slit. The variation trend of the yield strength of the core samples in the cutting direction and perpendicular to the cutting direction was analyzed by fitting the yield strength of the core samples and the distance from the center of the blast hole, as shown in Figure 6.

Figure 6 shows that the increasing distance from the center of the blast hole increases the growth rate of the yield strength of the core sample of 0.3422 in the cutting direction. The growth rate of the yield strength of the core sample perpendicular to the slit direction is 0.1291, and that of the core sample in the slit direction is greater than that of the core sample perpendicular to the slit yield strength.

4.2. The Effect of Rock Damage and the Blasthole Distance. The damage variable D [21, 22] is often used to describe the damage degree in the blasting process. $\Omega = 0$ and 1 represent the undamaged and completely damaged rocks, respectively. Therefore, taking the green sandstone without explosive loading as the benchmark, the core samples in the cutting direction and perpendicular to the cutting direction were analyzed based on the yield strength of the core samples in both directions. The damage degree and the distance from the center of the blasthole were fitted to reveal the relationship, and the damage degree of the core sample in the

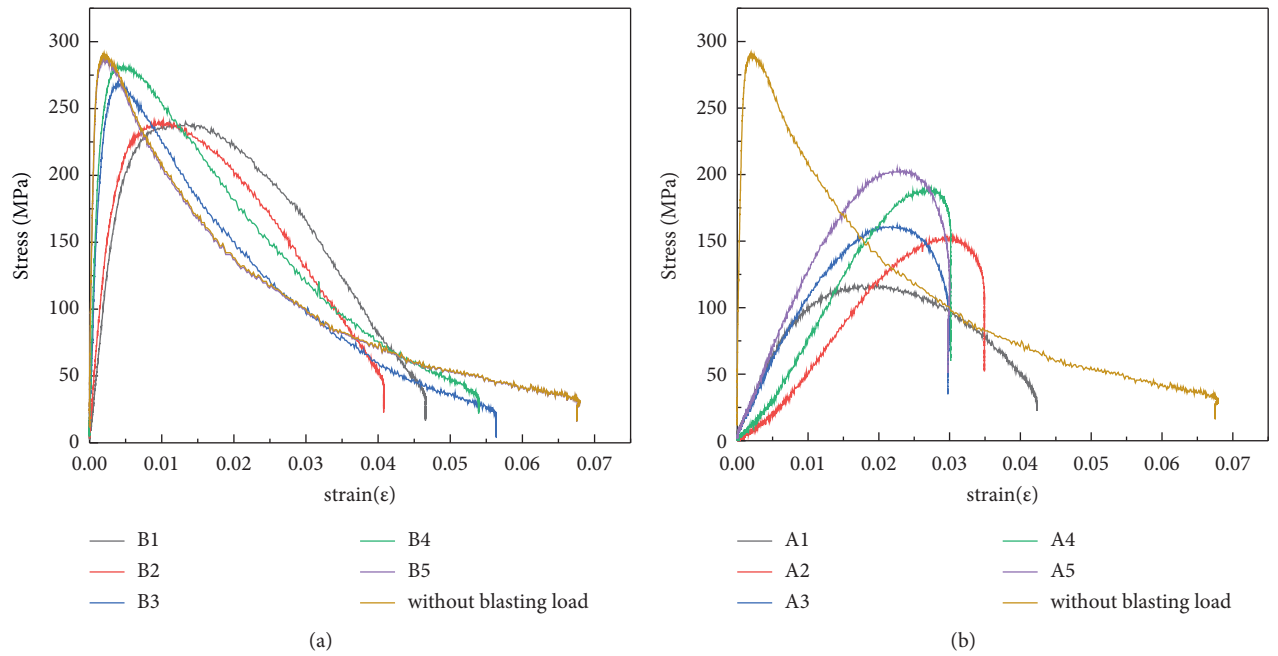

Figure 5: Stress-strain relationship curves of the core sample in the directions. (a) Perpendicular to the slit. (b) Parallel to the slit.

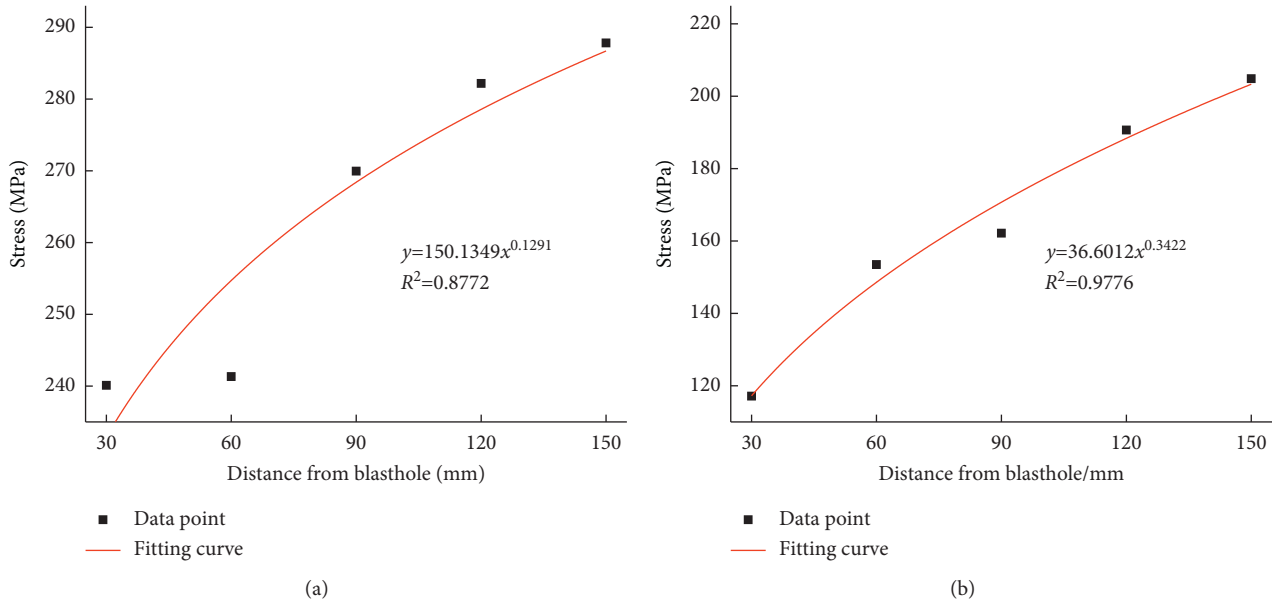

Figure 6: Fitting curves of yield strength and distance of specimen. (a) Vertical cutting direction. (b) Slitting direction.

direction of the slit and perpendicular to the direction of the slit is shown in Figure 7. The damage degree was calculated as follows:

$$\Omega = 1 - \frac{\sigma_{\max}}{\sigma_0}. \quad (1)$$

Figure 7 shows the fitting curve of the relationship between the damage degree of the sample and the distance from the center of the blasthole. The damage degree of the core sample perpendicular to the cutting direction and the direction of the cutting seam increases with increasing distance from the center of the blasthole. Moreover, the attenuation degree of the damage degree in the slit direction is significantly greater than that of the damage degree perpendicular to the slit direction. The minimum damage degree of the core sample in the cutting direction is greater than the maximum damage degree of the core sample perpendicular to the cutting direction.

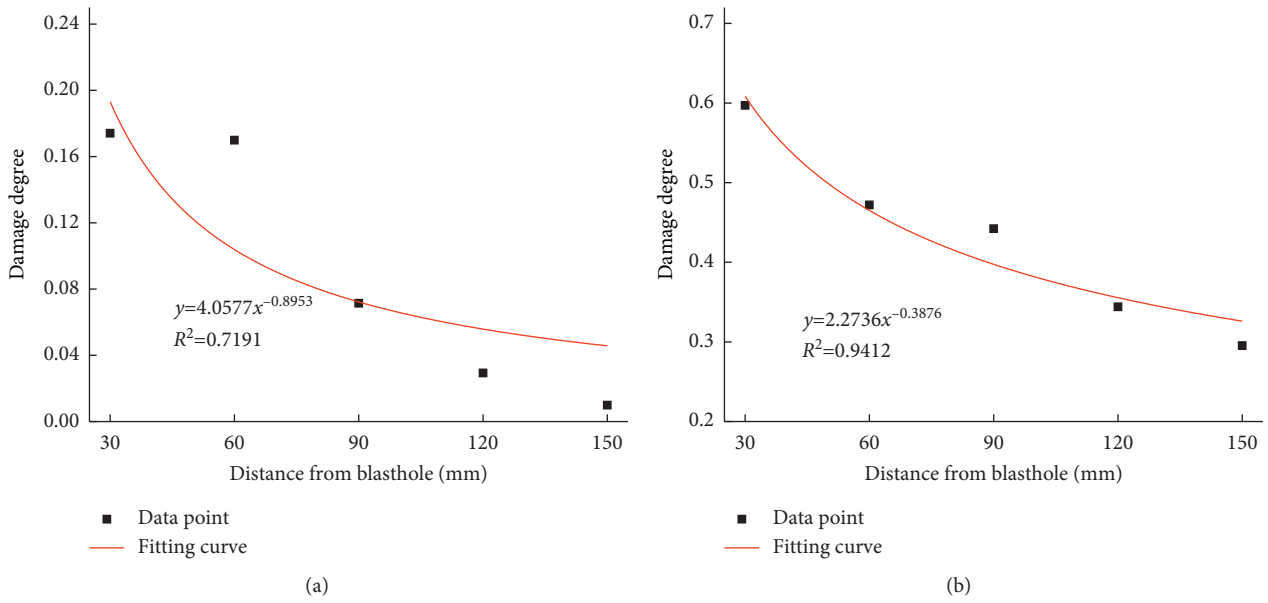

Figure 7: The fitting curve of damage degree and distance of specimen. (a) Vertical cutting direction. (b) Slitting direction.

4.3. Fractal Dimension Calculation of Block Degree. In the 1970s, Mandelbrot [23] proposed the concept of fractal theory. Xie et al. [24, 25] first applied fractal theory to rock mechanics and conducted in-depth research, indicating that the micro- and macro-mechanical responses of rocks (rock-like materials) exhibit strong mathematical and statistical self-similarity and have obvious fractal characteristics.

If the rock sample has a constant density of rock fragments, the mass of the fragments measured by the sieving method can be used to study the distribution law of the degree of fragmentation. The fractal dimension D is calculated using the mass of the fragments—equivalent particle size, represented [26] as follows:

$$D = 3 - \alpha,$$
$$\alpha = \frac{\lg(M(r)/M)}{\lg r}, \tag{2}$$

where α is the slope of $\lg(M(r)/M)$-$\lg r$ under the double logarithmic coordinate, r is the characteristic size of the equivalent particle size in the statistical interval and generally takes multiple intervals, M is the total mass of the fragments in the calculation scale, $M(r)$ represents the fragment mass whose equivalent particle size is smaller than r, and $M(r)/M$ is the cumulative percentage content of fragments whose equivalent particle size is less than r.

According to the above method for calculating the fractal dimension D, the broken pieces of the core sample can be weighed by the sieving method, and the mass percentage of the broken rock sample with a particle size smaller than r over the total rock mass was obtained. If the linear correlation of $\lg(M(r)/M)$ is high, it indicates that the size distribution of the fragments conforms to the fractal characteristics. If the linear correlation is poor, it indicates that the proportion of small size fragments is relatively large [27–29]. This method obtains the fractal dimension of the block degree $D = 0$–3, indicating that at $D = 2$, the mass ratio of fragments in each scale interval is equal to the fractal scale interval. Conditions $0 < D < 2$ and $2 < D < 3$ provide a larger mass proportion of fragments in the small-scale interval and a larger mass proportion of fragments in the large-scale interval, respectively.

The rock fragments in the above SHPB experiment were sieved and weighed. The data were used to study the effect of impact load on the fractal dimension and fractal characteristics of rock fragmentation distribution. According to the crushing characteristics of the sample, the characteristic sizes of the block fractal from small to large are 0.075, 0.425, 0.63, 1.2 5, 2.5, 5, 10, 15, 30 mm, and 40 mm. The sieved samples are shown in Figure 8, and their calculated masses are listed in Table 1.

Figure 9 shows the relationship diagram of $\lg(M(r)/M)$ and $\lg(r)$. The fracture distribution of the crushed specimens under the impact load shows a good statistical self-similarity. A good linear correlation was observed between $\lg(M(r)/M)$ and $\lg(r)$, exhibiting prominent fractal characteristics. Figure 9(a) shows the fitting results of the specimen perpendicular to the slit direction. The fitting slope α of the compared specimens is 0.7128, and the fractal dimension D calculated by equation (2) is 2.2872. The fitting slopes of specimens A1, A2, A3, A4, and A5 are 0.9795, 0.9743, 0.9377, 0.8706, and 0.7804, respectively, and the fractal dimensions DA1, DA2, DA3, DA4, and DA5 are 2.0205, 2.0257, 2.0623, 2.1294, and 2.2196, respectively. Figure 9(b) illustrates the fitting results of the specimens in the vertical slit direction. The fitting slopes of specimens B1, B2, B3, B4, and B5 are 1.6052, 1.1906, 1.1860, 0.9853, and 0.9841, respectively, and the fractal dimensions DB1, DB2, DB3, DB4, and DB5 are 1.3948, 1.8094, 1.814, 2.0147, 2.0159, respectively.

Figure 8: Screening diagram of crushed specimens.

Table 1: Fragment mass distribution of SHPB experimental specimens.

Characteristic size r (mm)	Rock fragmentation mass (g)									
	A1	A2	A3	A4	A5	B1	B2	B3	B4	B5
40	0	59	60.5	0	0	148.8	0	80	85.9	0
30	0	0	0	110.5	0	0	0	73.3	38.5	42.6
15	109.1	78.3	73.9	18.3	102.3	12.4	136.4	0	14.5	38.3
10	25.7	19.8	12.1	20.1	24.6	0	17	3.8	5.5	41.2
5	9.3	3	6.7	5.5	15.5	0.9	4.1	1.3	8.8	19.8
2.5	4.5	1.7	2.7	1.5	5	0	1.1	0.1	4.8	6.4
1.25	2.3	0.8	1.2	0.9	2.5	0	0.3	0.1	0.7	2.7
0.63	2	0.5	1	0.7	1.7	0.1	0.1	0.1	0.4	2.3
0.425	0.4	0.3	0.1	0.1	0.7	0	0.1	0.1	0.1	0.6
0.075	6	1.4	3.5	1.7	5.3	0	0.9	0.1	0.9	6.7
<0.075	0.1	0	0.1	0.3	0	0	0	0	0	0.1
Total mass	159.4	164.8	161.8	159.6	157.6	162.2	160	158.9	160.1	160.7

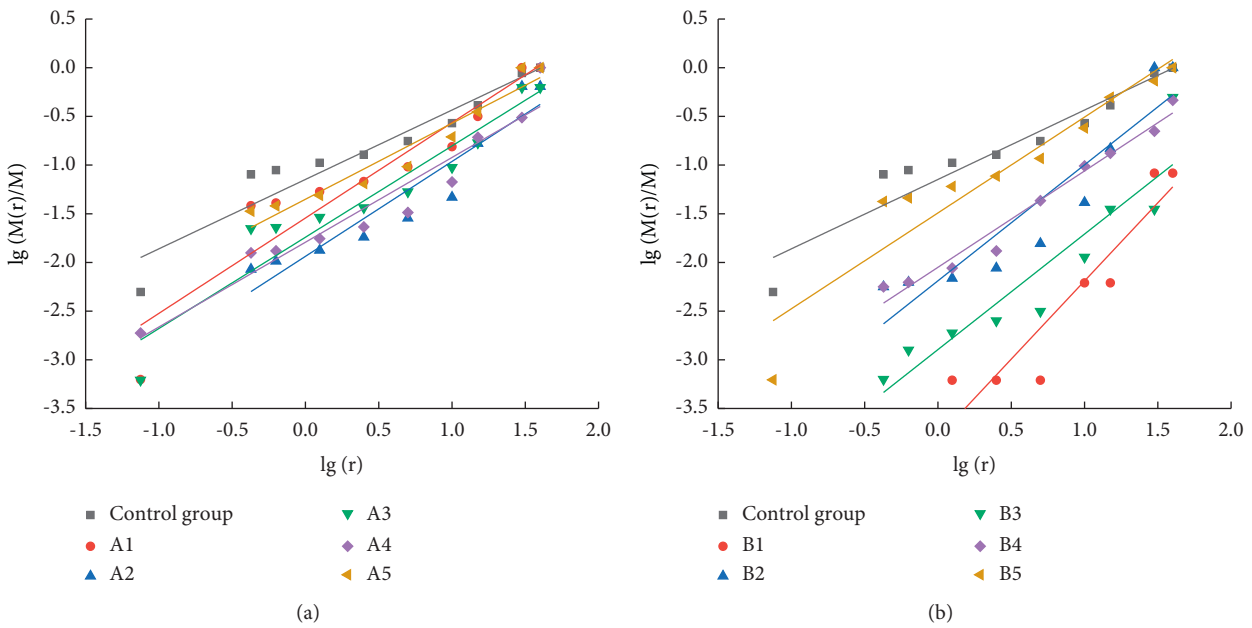

Figure 9: The fitting relationship between lg($M(r)/M$) and lg(r). (a) Perpendicular to the slit direction. (b) Parallel to the slit direction.

Figure 10 shows the fractal dimension curves at different distances. At a further distance from the core to the blast hole, the fractal dimension of the specimen after failure is larger, indicating that the degree of fragmentation of the specimen is smaller. The fractal dimension of the specimens perpendicular to the slitting direction at the same distance is larger than that of the specimens in the slitting direction, verifying the damage reduction effect of the slit charge.

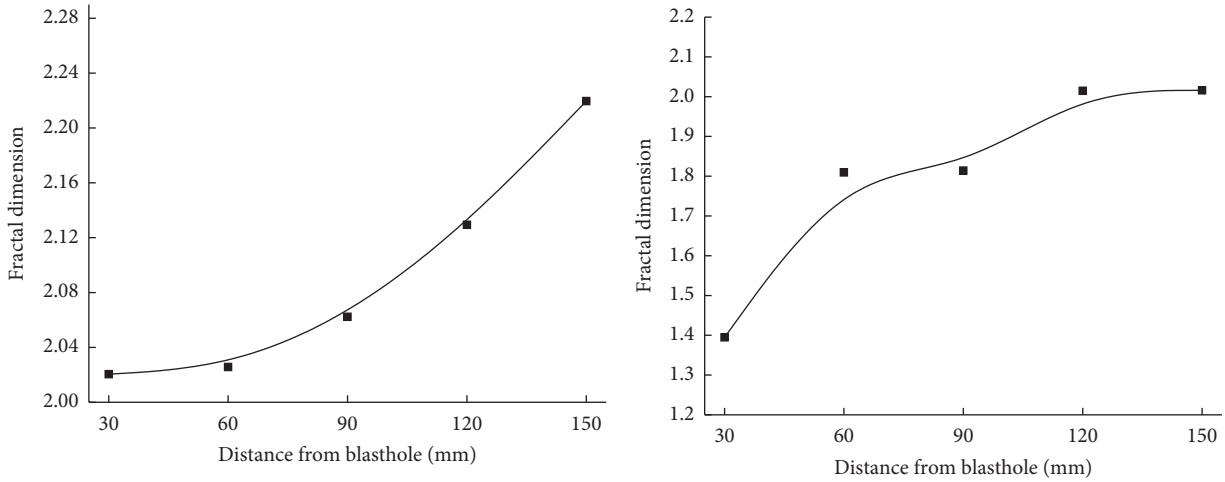

Figure 10: Fractal dimension curves at different distances. (a) Perpendicular to the slit direction. (b) Parallel to the slit direction.

5. Conclusion

Green sandstone was used as the experimental material to investigate the split-Hopkinson pressure bar experiment system for understanding the damage characteristics of the rock in the direction of the slit and the vertical direction of the slit after the blasting of the slit charge, leading to the following conclusions.

(1) The dynamic strength of the rock is defined as the damage degree of the rock. The damage degree of the rock in the direction of the slit is greater than that of the rock perpendicular to the direction of the slit. In the direction perpendicular to the slit direction, the rock damage characteristics at a distance of 150 mm from the blasthole are analyzed. The core is almost immune to blast loads.

(2) The damage degree of the rock in the kerf direction and perpendicular to the kerf direction attenuates exponentially with increasing distance from the blast hole, and the attenuation index −0.3876 of the damage degree in the kerf direction is significantly larger than that in the direction perpendicular to the kerf degree decay index of −0.8953.

(3) The block size distribution of rock specimens under impact load shows good statistical self-similarity. According to the evolution law of fractal dimension, the farther the core is from the blast hole, the greater the fractal dimension of the specimen is after failure. The fractal dimension (2.0205–2.2196) of the specimen perpendicular to the slit direction at the same distance is greater than that (1.3948–2.0159) of the specimen in the slit direction.

Data Availability

The data used to support the findings of this study are included within the article.

Conflicts of Interest

The authors declare that there are no conflicts of interest regarding the publication of this paper.

Acknowledgments

This study was supported by Natural Disaster Prevention, Equipment Research, and Application-Research and Development of Early Warning and Prevention Technology for Geological Disasters in Transportation Infrastructure (grant no. 2021KCKT2011) and Ministry of Natural Resources of the People's Republic of China (grant no. ZJDZGCZ-2021).

References

[1] Q. Wang, M. He, J. Yang, and H. Gao, "Study of a no-pillar mining technique with automatically formed gob-side entry retaining for longwall mining in coal mines," *International Journal of Rock Mechanics and Mining Sciences*, vol. 110, pp. 1–8, 2018.

[2] Q. Wang, Z. Jiang, and B. Jiang, "Research on an automatic roadway formation method in deep mining areas by roof cutting with high-strength bolt-grouting," *International Journal of Rock Mechanics and Mining Sciences*, vol. 128, p. 104264, 2018.

[3] W. L. Fourney, J. W. Dally, and D. C. Holloway, "Controlled blasting with ligamented charge holders," *International Journal of Rock Mechanics and Mining Science & Geomechanics Abstracts*, vol. 15, no. 3, pp. 121–129, 1978.

[4] W. L. Fourney, D. B. Barker, and D. C. Holloway, "Model studies of well stimulation using propellant charges," *International Journal of Rock Mechanics and Mining Sciences & Geomechanics Abstracts*, vol. 20, no. 2, pp. 91–101, 1983.

[5] J. W. Dally and W. L. Fourney, *Fracture Control in Construction Blasting*, in *Proceedings of the 18th U.S by Symposium on Rock Mechanism*, ColoradoARMA-77-0101, Colorado, June 1977.

[6] Z. Tang and Z. Xiao, "Study on stress distribution law of slit charge blasting," *Sichuan Metallurgy*, vol. 3, pp. 2–5, 1997.

[7] X. Gao, *Detonation Shock Dynamic Behavior of Split-Tube Charge Holder [PhD Thesis]*, China University of Mining and Technology, Beijing), Beijing, 2009.
[8] S. Wang and Y. Wei, "Fracture control in rock blasting," *Journal of China University of Mining and Technology*, vol. 3, pp. 118–125, 1985, (In Chinese).
[9] Y. Yang, Q. Gao, and M. Yu, "Experimental study of mechanism and technology of directed crack blasting," *Journal of China University of Mining and Technology*, vol. 5, no. 2, pp. 69–77, 1995.
[10] R. Yang, J. Zhuang, and W. Wang, "Application of directional broken control blasting in cutting," *Journal of China University of Mining and Technology*, vol. 10, no. 2, pp. 7–10, 2000.
[11] J. Song and R. Yang, "Model test research on blasting parameters and stress field of slotted holes," *Mine Construction Technology*, vol. 01, pp. 23–27, 1997, (In Chinese).
[12] R. Yang, J. Song, and Y. Yang, "Model test research on blasting mechanism of slotted holes," *Journal of China Coal Society*, vol. 20, no. 02, pp. 197–200, 1995, (in Chinese).
[13] L. Yu, H. Su, and R. Liu, "Experimental study of the influence of loading rate on tensile mechanical behavior of sandstone damaged by blasting," *Arabian Journal of Geosciences*, vol. 10, no. 19, pp. 1–12, 2017.
[14] J. Wang, T. Zuo, and X. Li, "Study on the fractal characteristics of the pomegranate biotite schist under impact loading," *Geofluids*, vol. 2021, p. 1570160, 2021.
[15] Q. Wang, Y. Wang, and M. He, "Experimental research and application of automatically formed roadway without advance tunneling," *Tunnelling and Underground Space Technology*, vol. 114, p. 103999, 2021.
[16] Q. Wang, M. He, and S. Li, "Comparative study of model tests on automatically formed roadway and gob-side entry driving in deep coal mines," *International Journal of Mining Science and Technology*, vol. 114, p. 103999, 2021.
[17] Q. Wang, P. Zhang, and Z. Jiang, "Automatic roadway formation method by roof cutting with high strength bolt-grouting in deep coal mine and its validation," *Journal of China Coal Society*, vol. 46, no. 02, pp. 382–397, 2021, (In Chinese).
[18] J. Dai, *Rock Dynamics and Blasting Theory*, Metallurgical Industry Press, Beijing, China, 2002.
[19] Q. Ma, J. Song, and D. Ma, "SHPB experimental study on dynamic characteristics and failure behaviors of sandstone containing weakly filled joints with various angles in deep roadways," *Chinese Journal of Rock Mechanics and Engineering*, vol. 39, no. 06, pp. 1104–1116, 2020, (In Chinese).
[20] H. Meng and Q. M. Li, "Correlation between the accuracy of a SHPB test and the stress uniformity based on numerical experiments," *International Journal of Impact Engineering*, vol. 28, no. 05, pp. 537–555, 2003.
[21] Z. Wang, H. Wang, and J. Wang, "Finite element analyses of constitutive models performance in the simulation of blast-induced rock cracks," *Computers and Geotechnics*, vol. 135, p. 104172, 2021.
[22] L. X. Xie, Q. B. Zhang, and J. C. Gu, "Damage evolution mechanism in production blasting excavation under different stress fields," *Simulation Modelling Practice and Theory*, vol. 97, p. 101969, 2019.
[23] B. B. Mandelbrot, *The fractal geometry of nature*, Shanghai far East Publishing House, Shanghai, 1998.
[24] H. P. Xie, F. Gao, and Y. Ju, "Research and development of rock mechanics in deep ground engineering," *Chinese Journal of Rock Mechanics and Engineering*, vol. 34, pp. 2161–2178, 2015, (in Chinese).
[25] M. Z. Gao, J. Xie, J. Guo, Y. Q. Lu, Z. Q. He, and C. Li, "Fractal evolution and connectivity characteristics of mining-induced crack networks in coal masses at different depths," *Geomechanics and Geophysics for Geo-Energy and Geo-Resources*, vol. 7, no. 1, p. 9, 2021.
[26] T. Deng, L. Yang, and W. Han, "Influence of loading form on distribution of marble fragments," *Journal of Tongji University*, vol. 35, no. 01, pp. 10–14, 2007, (in Chinese).
[27] C. Zhu, M. C. He, B. Jiang, X. Z. Qin, Q. Yin, and Y. Zhou, "Numerical investigation on the fatigue failure characteristics of water-bearing sandstone under cyclic loading," *Journal of Mountain Science*, vol. 18, no. 12, pp. 3348–3365, 2021.
[28] Y. Wang, H. N. Yang, J. Q. Han, and C. Zhu, "Effect of rock bridge length on fracture and damage modelling in granite containing hole and fissures under cyclic uniaxial increasing-amplitude decreasing-frequency (CUIADF) loads," *International Journal of Fatigue*, vol. 158, p. 106741, 2022.
[29] Z. J. Wu, Z. Y. Wang, L. F. Fan, L. Weng, and Q. S. Liu, "Micro-failure process and failure mechanism of brittle rock under uniaxial compression using continuous real-time wave velocity measurement," *Journal of Central South University*, vol. 28, no. 2, pp. 556–571, 2021.